DOI: 10.17580/cisisr.2020.01.10

HOT PHYSICAL SIMULATION OF δ-FERRITE BEHAVIOR AT PRODUCTION AND WELDING OF HIGH-NITROGEN CORROSION-RESISTANT STEELS

A. A. Kazakov[1], A. I. Zhitenev[1], P. A. Ishpaev[1], O. V. Fomina[2], P. V. Melnikov[2]

[1] *Peter the Great St. Petersburg Polytechnic University (St. Petersburg, Russia)*
[2] *National Research Center "Kurchatov Institute" — Central Research Institute of Structural Materials "Prometey" (St. Petersburg, Russia)*

E-mail: kazakov@thixomet.ru; zhitenev@thixomet.ru

AUTHOR'S INFO

A. A. Kazakov, Dr. Eng., Prof., Head of "Metallurgical Examination" Lab.,
A. I. Zhitenev, Engineer, "Metallurgical Examination" Lab.,
P. A. Ishpaev, Magister, "Metallurgical Examination" Lab.,
O. V. Fomina, Dr. Eng., Head of the Research and Production Complex "Organization and Management of R&D, Computer Science and Computer Technology, Quality Management and Copyright Protection",
P. V. Melnikov, Cand. Eng., Head of Department

Key words:
corrosion-resistant austenitic steels, δ-ferrite, volume fraction, morphology, thermodynamic criteria, hot physical simulation.

ABSTRACT

The thermodynamic criteria previously proposed for interpretation of the origin of δ-ferrite in high-strength corrosion-resistant austenitic steels were enhanced by results obtained after hot physical simulation. Combination of these approaches enabled understanding of the details of the behavior of δ-ferrite during solidification and cooling of the solid steel, and to ensure its hot-cracking resistance in the presence of the optimum amount of δ-ferrite during hot plastic deformation or welding, as well as subsequent austenitization of the structure to minimize or eliminate δ-ferrite in the finished metal.

The compositions of steels for studying the behavior of δ-ferrite were selected based on previously developed thermodynamic criteria. It was shown that the δ-ferrite fraction retained in cast metal was determined not only by these criteria characterizing its thermodynamic stability during solidification of liquid and cooling solid steel, but also by its cooling rates in the temperature ranges of δ-ferrite and austenite existence.

The mechanism and conditions for δ-ferrite formation of globular, lacy or vermicular morphology depend on the steel composition and its cooling rate which has been revealed when analyzing experimental results of hot physical simulation.

All the results obtained are summarized by a regression equation that adequately describes the effect of the steel composition and its cooling rate on the δ-ferrite fraction retained in the finished metal.

Introduction

The production of high-strength corrosion-resistant austenitic steels is associated with a constant search for compromised solutions. On the one hand, the production of non-magnetic steel requires a stable uniform austenitic structure [1, 2]; on the other hand, steels with such structure are sensitive to hot cracking during hot plastic deformation [3] and welding [4, 5]. Crystallization through δ-ferrite and its presence in optimal amount at hot deformation and welding enables to significantly increase a steels hot cracking resistance [6–9]. However, δ-ferrite retained in the finished metal can make it unsuitable for a wide range of applications.

Typically, the retained δ-ferrite fraction is predicted by the empirical Schaeffler diagram [10] or its modifications [11–14]. However, the whole variety and completeness of as-cast steel structure formation processes are not fully taken into account in these diagrams [6, 7]. Earlier, thermodynamic criteria were proposed that could interpret the origin of δ-ferrite in nitrogen [14] and chromium steels [15] to predict their retained δ-ferrite amount. However, using only the thermodynamic approach is insufficient to understand the δ-ferrite distribution, including its morphology, over the cross section of an ingot or weld [16, 17]. These processes depend on the actual cooling conditions of the steel during its solidification and subsequent cooling in the solid state.

Therefore, the goal of this paper is to develop δ-ferrite origin controlling methods on the basis of the results obtained by hot physical simulation interpreted by thermodynamics.

Materials and methods

Specimens of austenitic and austenitic-ferritic corrosion-resistant steels were made in an open induction furnace with a capacity of 20 kg and were investigated. Hot physical simulation of their crystallization process for the main metal was carried out on the basis of steel grade 0.04C20Cr6Ni11Mn2MoNVNb [1] and for the welding materials based on EP 647 welding wire grade C0.1Cr19Ni11Mn4Mo [2, 18]. Pure raw materials were used: electrical steel, metallic manganese (Mn95), metallic chromium (Cr100), cathode nickel, ferromolybdenum (FeMo65), ferroniobium (FeNb70), ferrovanadium (FeV80), and nitrogenous ferrochrome (FeCrN10).

After the raw materials were melted and all alloying elements were added, the steel was discharged into a tundish, from which it was poured into copper and cast iron molds, as well as into three identical sand molds, two ingots of which after solidification were quenched from different temperatures. Thus, five ingots were made of the

Table 1. **Chemical composition of experimental steels**

Steel	Elements, wt.%								
	C	Si	Mn	Cr	Ni	Mo	Cu	Ti+Nb+V	N
1	0.05	0.5	10	21	5	1.5	0.1	0.1	0.45
2	0.07	0.65	1.65	16.8	11.2	3.5	0.16	0.05	0.148
3	0.06	0.5	1.7	21.2	9.9	5.2	0.18	0.05	0.112

same size (110-mm high and 40-mm in diameter) and weight (1 kg each) with the same chemical composition, but were crystallized and cooled down at different rates.

Ingots with different contents of Cr, Ni, and Mo, but with the same composition of the remaining metal matrix, were made by fractional casting [13–15]. The temperature of the molten metal at casting was kept constant, controlling it with an immersion WRe5/20 thermocouple, equipped with a single-channel recording device with automatic compensation of the cold junction temperature. The same thermocouple was installed in the geometrical center of the sand mold to record the steels cooling curve during solidification.

The experimental steel compositions were determined with a SPECTROMAX-F optical emission spectrometer (**Table 1**).

Specimens were cut from the ingots at a distance of 30-mm from the bottom, and then they were mounted into a phenolic compound, ground and polished using Buehler equipment and their metallographic consumables. Then, the specimens were removed from the compound and etched electrolytically in a 60% aqueous nitric acid solution for 15 seconds. Such etching reveals the δ-ferrite retained in steel, the volume fraction and morphology of which was examined using a Zeiss Axiovert 200 MAT metallographic microscope equipped with a Thixomet Pro image analyzer [19]. The measurements were performed on panoramas with an area of 3.4 mm^2, created at a magnification of ×200. Three panoramas, made at a distance of 2, 8 and 12 mm from the edge of the ingot, were studied on each cross section.

Thermodynamic simulation was performed using FactSage commercial software equipped with SGTE databases [20]. Solidification calculations were carried out according to the lever rule. To study the crystallization and solidification kinetics, as well as the subsequent cooling of solid steel, the PolyCast software package was used [21]. Multivariate regression analysis of experimental data was performed using the Statistica software.

Thermodynamic behavior criteria for δ-ferrite

The compositions of steels for a detailed study of δ-ferrite behavior were selected according to the results of thermodynamic simulation (**Fig. 1**) based on previously developed criteria [14, 15]:

ΔT_δ and ΔT_{tech} — temperature intervals of δ-ferrite existence during solidification and below the solidus temperature, correspondingly;

ΔT_γ — temperature interval of austenite field where metastable δ-ferrite, retained after solidification and further cooling of solid steel below interval ΔT_{tech}, completely transforms into austenite [10, 13, 14];

Δ(δ) — depth of the δ-ferrite transformation [15], calculated as an area under the graph "δ-ferrite fraction versus temperature" (see Fig. 1).

The simulation results analysis for the nitrogen-enhanced steel 1 based on the grade C0.04Cr20Ni6Mn11Mo2NNbV (see Fig. 1, *a*) shows that there is a large depth of δ-ferrite transformation Δ(δ) to ensure these steels have hot-cracking resistance during hot plastic deformation [6, 7], but at the same time there is a wide interval $\Delta T\gamma$ for its subsequent austenitization.

The δ-ferrite behavior was also studied using the welding consumables [15], formally related to steel C0.1Cr19Ni11Mo4V (wire EP-647), but with different contents of molybdenum, nickel and nitrogen within this grade (see Fig. 1, *b*).

For steels containing 11% nickel and 3.3% molybdenum (curve *2* in Fig. 1, *b*), the maximum equilibrium temperature of austenitization is too low (1240 °C) even though the depth of the δ-ferrite transformation Δ(δ) is small. This means that such a steel has all the advantages of crystallization through δ-ferrite and will provide a weld without hot cracks [8, 9], but its formation of austenite during natural cooling can be a problem.

In the steel containing 10% Ni and 5.2% Mo (curve *3* in Fig. 1, *b*), the depth of the δ-ferrite transformation Δ(δ) is larger, and the temperature range of austenitization $\Delta T\gamma$ is completely absent. Moreover, σ-phase is formed in this steel [22]. Therefore, the δ-ferrite fraction in such steels at high temperatures is excessive, austenitization is impossible, and the presence of σ-phase makes it completely unsuitable for welding.

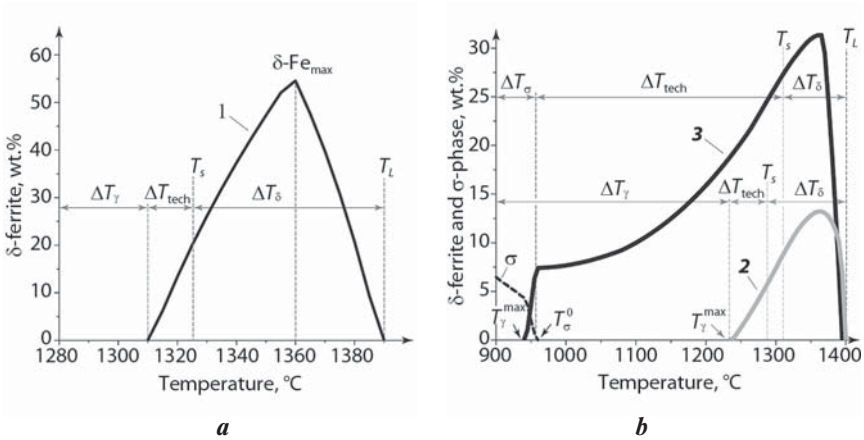

a *b*

Fig. 1. Behavior of δ-ferrite during crystallization, solidification and cooling of solid nitrogen steel 1 (*a*) and Cr-Ni-Mn steel 2 and steel 3 (*b*)

Retained δ-ferrite content in the finished metal

The criteria discussed above are based on equilibrium simulation results, which should be correctly interpreted to describe real metallurgical processes running at finite cooling rates. It will be illustrated how to take into account the kinetics of crystallization and solidification processes, using equilibrium calculations along with hot physical and thermophysical simulation approaches.

The thermophysical simulation was carried out on the basis of the PolyCast software package and compared with thermal curves obtained experimentally with steels solidified in sand molds (**Fig. 2**). The experimental curve clearly fixes the inflections responsible for the δ-ferrite crystallization, as well as the beginning and the end of the peritectic reaction, that coincide with the results of thermodynamic (see Fig. 1, *a*) and thermophysical simulations (curve *2* in Fig. 2).

As follows from the hot simulation summary (**Fig. 3**), the cooling rate and local solidification time vary significantly over the cross section of the ingot in cast iron and; especially, in copper molds. The cooling rate along the ingot cross section varies insignificantly in the sand mold, and the local solidification time is many times longer unlike metal molds.

Despite such a difference in the cooling rates of steel in metal and sand molds, the δ-ferrite fraction and its distribution over the cross section of all ingots are approximately the same and could be described by one line 1 in **Fig. 4**.

The δ-ferrite fraction grows linearly from the edge to the center of all ingots made from steel 1. Taking into account the precision of measurements, the volume fractions of δ-ferrite obtained at the same points of the ingots cast in metal and sand molds are very close. In other words, the cooling rate during solidification and cooling of steel in solid state is not critical for the δ-ferrite fraction retained in the finished ingots.

This is explained by the fact that, when casting into metal molds, due to the high cooling rates of the melt at the liquidus temperature (2–13 °C/s), the δ-ferrite fraction is significantly below the equilibrium one, because it does not have time to form to the full extent due to fast solidification [23, 24]. The same high cooling rates are maintained in the solid metal in the range of ΔT_{tech} (7–12 °C/s) and ΔT_{γ} (~5 °C/s), which prevents the complete transform of δ-ferrite to austenite [25]. Upon slow cooling of the melt in the sand mold (0.7–0.8 °C/s), the δ-ferrite fraction formed during crystallization approaches equilibrium, but upon subsequent slow cooling of the solid metal in the range of ΔT_{tech} (1.6–2.4 °C/s) and ΔT_{γ} (~1.2 K/s) it is almost completely transformed into austenite. Therefore, at the same points of the ingots obtained in metal and sand molds, approximately the same fraction of retained δ-ferrite was revealed.

Steel 1 was cast into three identical sand forms, two ingots of them after solidification were quenched from different temperature. The higher the temperature at which the ingot was quenched, the more δ-ferrite remained in it that was not austenitizied. In the center of the ingots, the volume fraction of retained δ-ferrite decreases from 4.5–3.5 vol.% when quenched after casting within 2–3 minutes correspondingly to 2.5 vol.% if the ingot is naturally cooled in air in a sand mold.

The linear δ-ferrite fraction distribution over the cross section of the ingot was also revealed in Cr–Ni–Mo steels based on EP 647 welding wire (curves 2 and 3, Fig. 4). These results should be considered taking into account the thermodynamic features of the δ-ferrite formation in steels of different compositions (see Fig. 1, *b*).

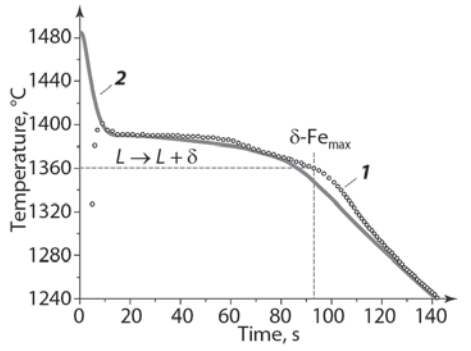

Fig. 2. Experimental (*1*) and calculated (*2*) thermal curves for the solidification of steel 1 in the sand mold

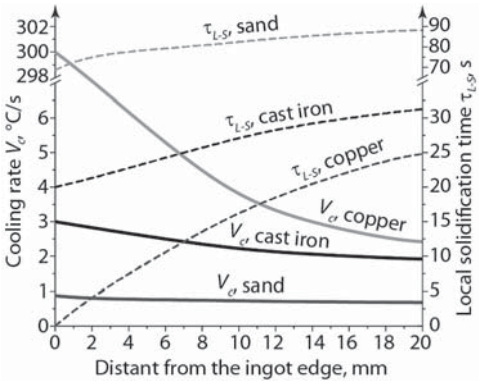

Fig. 3. Cooling rate and local solidification time over the cross section of ingots obtained in metal and sand molds

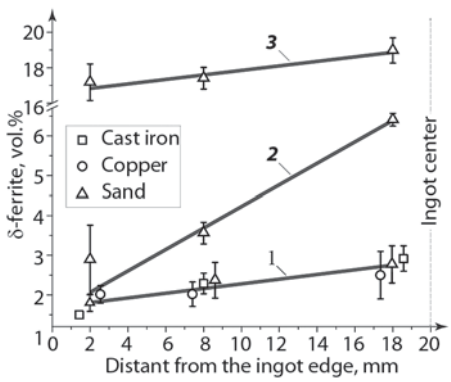

Fig. 4. Distribution of δ-ferrite over the cross section of ingots cast in metal (copper or cast iron) and sand molds for steel 1 (*1*), steel 2 (*2*) and steel 3 (*3*)

The depth of the δ-ferrite transformation Δ(δ) in steel 2 is less than that of steel 1; nevertheless, the maximum austenitization temperature is the decisive factor determining the δ-ferrite fraction retained in the finished metal (see Fig. 1). Thus, upon cooling down to 1310 °C, while the high diffusion mobility of atoms still remains [14, 25], steel 1 is being actively austenitized (see Fig. 1, *a*), while at the same temperature, steel 2 still contains at least 5 wt.% of equilibrium δ-ferrite (see Fig. 1, *b*).

So, more δ-ferrite was found in the ingot of steel 2 and the difference increased from the edge of the ingot to its center. In the same direction, the cooling rate of steel decreases; therefore, δ-ferrite forms more fully during its crystallization and solidification. With a decrease in the cooling rate in the solid metal, the steel should be fully austenitized, if thermodynamic conditions allow. Exactly because of this reason, in steel 1, the retained δ-ferrite fraction is smaller and it is more uniformly distributed over the cross section of the ingot (see Fig. 4). The thermodynamic condition of austenitization of steel 2 is satisfied only at temperatures below 1200 °C (see Fig. 1, *b*), where the diffusion mobility of atoms is suppressed [14, 25, 26]. Therefore, in steel 2, in the absence of austenitization, the ascending straight line of the retained δ-ferrite distribution from the edge to the center of the ingot reflects the increasing completeness of its formation during crystallization.

Three times more δ-ferrite fraction is formed in the center of the steel 3 ingot than in the same location of steel 2, and it is uniformly distributed over its cross section. Such a high δ-ferrite fraction, and the its uniform distribution, is explained by the large depth of the δ-ferrite transformation Δ(δ) of this steel in the complete absence of its austenitization interval $\Delta T\gamma$ (see Fig. 1, *b*).

Thus, the retained δ-ferrite fraction in the cast metal is determined by the thermodynamic criteria (ΔT_δ, ΔT_{tech}, ΔT_γ, Δ(δ)) and steel cooling rates in the temperature ranges of δ-ferrite (ΔT_δ and ΔT_{tech}) and austenite (ΔT_γ) existence. The cumulative knowledge of thermodynamic and kinetic behavior of δ-ferrite creates targeted control of technological parameters to ensure hot- cracking resistance of steel in the presence of the optimum δ-ferrite fraction during hot plastic deformation and welding; it also ensures achievement of subsequent austenitization of the structure to minimize or eliminate δ-ferrite in the finished metal.

Morphology of δ-ferrite

During the crystallization of steels through δ-ferrite, its morphology, depending on the cooling conditions, can vary from globular to lacy or vermicular [16–17, 24, 27 29].

At the beginning of crystallization, primary δ-ferrite dendrites are formed. If the cooling rate of the melt at the liquidus temperature is high, the δ-ferrite does not have enough time to fully form due to a slip through the onset crystallization temperature (see Fig. 1), and that high super cooling rates lead to formation of fine equiaxed branches of δ-ferrite [28, 30]. With further slow cooling, δ-ferrite easily spheroidizes, and its morphology becomes globular [27].

With a decrease of the cooling rate at the onset of the crystallization temperature, the thickness of the axes and the degree of branching increase. If upon further cooling of the ingot, there is not enough time for complete spheroidization, then partially spheroidized branched dendritic structures form the vermicular morphology of δ-ferrite [27, 29].

With very slow solidification, massive δ-ferrite dendrites are formed in the center of the ingot, which do not have time to transform into austenite in the solid metal. Due to the known features of the solid-phase transformation of ferrite–austenite [31], this metastable δ-ferrite is transformed into δ-ferrite with lacy morphology. With slow cooling below the solidus [25], or with isothermal holding in the austenitization interval $\Delta T\gamma$ [14, 26], both lacy and vermicular ferrite can be spheroidized by the reactive mechanism of Ostwald ripening [32, 33].

Fig. 5 shows the microstructures of ingot 1 cast in a copper mold with different δ-ferrite morphology, evolving from globular at the ingot edge (see Fig. 5, *a*) and vermicular at mid-radius (see Fig. 5, *b*) to lacy morphology in the center of the ingot (see Fig. 5, *c*). Such a distribution of the δ-ferrite morphological forms is in full accordance with the mechanisms of its formation stated above and known from the literature [10, 13, 14, 25–29].

The patterns of evolution of the morphology of δ-ferrite over the cross section of an ingot of welding materials (see Fig. 5, *d–i*) are similar to those found for the base metal.

In steel 2 with a small depth of the δ-ferrite transformation and a limited austenitization interval (see Fig. 1, *b*), the morphology of δ-ferrite from the surface to the center also changes from globular (see Fig. 5, *d*) to vermicular (see Fig. 5, *e*) and further to lacy (see Fig. 5, *f*). However, lacy δ-ferrite in the welding consumables has a much more developed morphology than in the base metal, since its fraction in these materials is substantially greater due to the low starting temperature of the austenitization.

Fig. 1, *b* shows that when steel 3 solidifies, more δ-ferrite is formed than in steel 2; therefore, in absence of deep supersaturations, the globular ferrite is not formed here [30]. There is practically no vermicular δ-ferrite here either, since there is no austenitization interval in this steel. For the same reason, the whole δ-ferrite remains in solid steel in a metastable state and, according to known patterns [31], acquires a developed lacy morphology. Exactly this type δ-ferrite was found over the entire cross section of the steel 3 ingot (see Fig. 5, *g–i*).

The ingot from a cast-iron mold shows the same patterns of the δ-ferrite formation of different morphology as found in the ingot from a copper mold.

In steel 1, cast in a sand mold, the δ-ferrite morphology over the cross section of the ingot almost does not change (**Fig. 6, *a–c***). Only δ-ferrite of vermicular morphology is found practically everywhere. A little

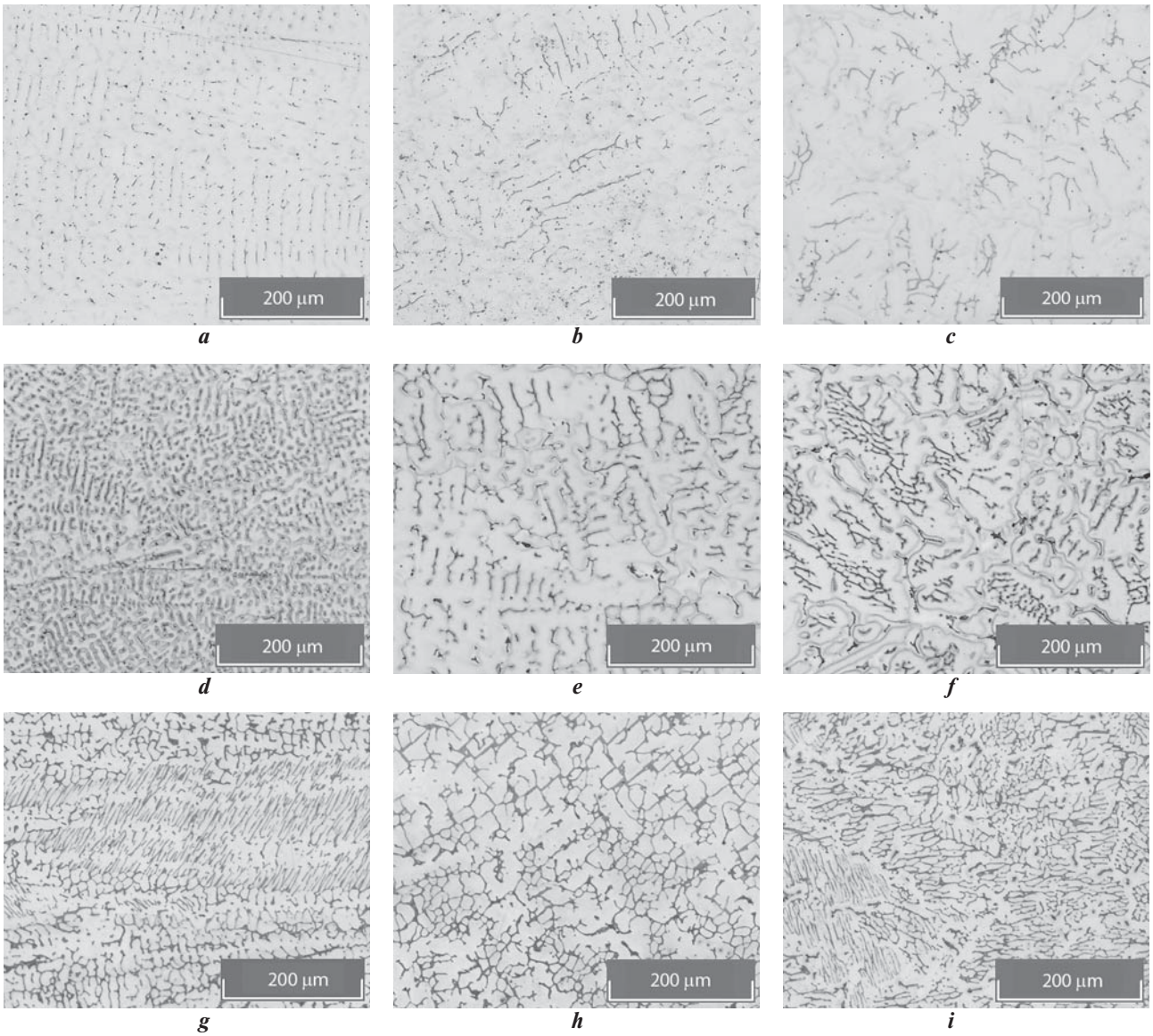

Fig. 5. Evolution of the morphology of δ-ferrite in ingots cast in a copper mold:
a, b, c — steel 1; *d, e, f* — steel 2; *g, h, i* — steel 3; *a, d, g* — edge; *b, e, h* — half the radius; *c, f, i* — center of the ingot

percentage of globular δ-ferrite was found on the edge of the ingot, and a little lacy - in its center. During solidification in the sand mold, in comparison with metal molds, the cooling rates are lower and approximately the same over the entire cross section of the ingot (see Fig. 3). At slow cooling rates, the metastable δ-ferrite does not remain in the solid metal; therefore, in the ingot cast in the sand mold, δ-ferrite of lacy morphology does not form.

The formation mechanisms of different morphologies of δ-ferrite are also confirmed in experiments with the ingot cast in the sand mold and then quenched after 2 and 3 minutes (see Fig. 6, *d–i*). After such quenching, a large amount of metastable δ-ferrite of lacy morphology was formed in the center of the ingot. In this case after quenching after 2 minutes of solidification (see Fig. 6, *f*), the amount and branching of the δ-ferrite of this morphology is noticeably higher compared to quenching from lower temperatures 3 minutes after casting (see Fig. 6, *i*). Quenching at higher temperatures leads to more deep supersaturation and more active metastable δ-ferrite formation.

The vermicular morphology δ-ferrite, found predominantly near the surface and in the middle of the radius of the quenched ingots because it formed upon slow cooling, sufficient for partial spheroidization of dendritic branches, but insufficient for their complete globularization. During natural cooling in a sand mold, only vermicular δ-ferrite is formed over the entire cross section of the ingot, since metastable δ-ferrite is not formed due to the slow cooling rate of the steel (see Fig. 6).

Prediction of retained δ-ferrite fraction in steel

While carrying out this work, we estimated the δ-ferrite fractions retained in steels with the same chemical composition, but crystallized and cooled at different cooling rates, as well as steels with different

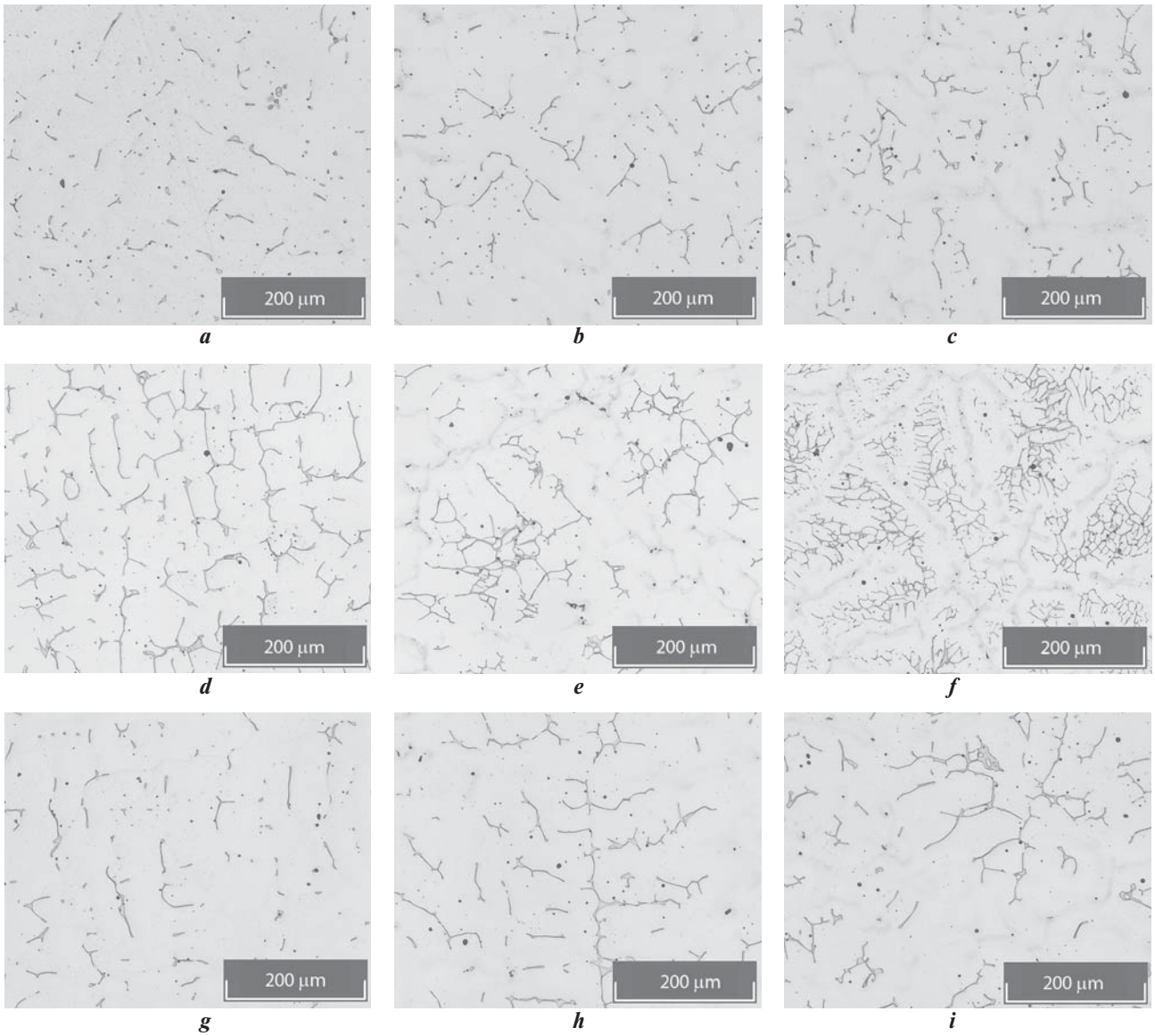

Fig. 6. Evolution of the δ-ferrite morphology in an ingot of steel 1 cooled with a sand mold (*a, b, c*) and quenched after 2 (*d, e, f*) and 3 (*g, h, i*) minutes:
a, d, g — edge; *b, e, h* — half the radius; *c, f, i* — center of the ingot

contents of Cr, Ni, and Mo with the same composition of the remaining metal matrix, made with known cooling rates. Using regression analysis, multidimensional models were constructed that adequately describe the retained δ-ferrite fraction considering the composition of the steel and its cooling rate:

$$V_\delta = -28 + 2.2\%\mathrm{Cr} + 1.4\%\mathrm{Mo} - 0.9\%\mathrm{Ni} - 0.13V_c; \quad (1)$$

$$V_\delta = -25 + 1.83\mathrm{Cr}_{eq} - 0.8\mathrm{Ni}_{eq} - 0.14V_c; \quad (2)$$

$$\mathrm{Cr}_{eq} = \mathrm{Cr} + 1.5\mathrm{Mo} + 1.5\mathrm{W} + 0.48\mathrm{Si} + 2.3\mathrm{V} + 1.75\mathrm{Nb} + 2.5\mathrm{Al}; \quad (3)$$

$$\mathrm{Ni}_{eq} = \mathrm{Ni} + \mathrm{Co} + 0.1\mathrm{Mn} - 0.01\mathrm{Mn}^2 + 18\mathrm{N} + 30\mathrm{C}. \quad (4)$$

In equation (1) used to estimate V_δ the weight % of alloying elements were used, and in equation (2) the chromium and nickel equivalents calculated by formulas (3) and (4) were used [12].

For each coefficient in equations (1) and (2) the p-value was below 0.05. **Fig. 7** shows a scattering diagram for δ-ferrite volume fraction calculated by these equations and measured experimentally. This diagram illustrates the high adequacy of regression equations (1) and (2): the determination coefficient $R^2 > 0.9$.

Let us verify how these equations describe other data, in particular, those known from the literature [34] and obtained for similar compositions of welding consumables at a cooling rate of $V_c = 10$ °C/sec. If the concentration of the alloying elements in the steel are expressed in wt.%, then all the points V_δ calculated according to equation (1) lie along the approximating curve 1:1, although published literature data have a wider degree of scatter than the data obtained in this paper (see Fig. 7, *a*). If the concentrations of the alloying elements are expressed in chromium and

nickel equivalents, then a systematic error occurs in the description of the literature data [34] by the equation (2): the approximating straight line deviates from the 1:1 line to the δ-ferrite axis (see Fig. 7, *b*), giving significantly underestimated forecasts for the δ-ferrite fraction. For half of these data, where the experimental fraction of δ-ferrite varies from 1 to 17%, the calculation gives zero forecasts (see Fig. 7, *b*).

This error is due to the fact that the same Cr_{eq} and Ni_{eq} can be obtained by a set of different concentrations of the same alloying elements. For example, in the steels of the 0.05C–0.2Si–11Mn–18.5Cr–1.3Mo–0.15Nb–0.15V system, the same Cr_{eq} = 21.35 and Ni_{eq} = 17.55 can be provided with three different concentrations of nitrogen and nickel (wt.%): 1) N = 0.45 and Ni = 8; 2) N = 0.51 and Ni = 7; 3) N = 0.62 and Ni = 5. As follows from thermodynamic simulation, during crystallization there is absolutely no δ-ferrite in the first steel, in the second one its fraction does not exceed 0.2%, and in the third one - more than 50% of δ-ferrite. Obviously, there will be no δ-ferrite retained in the first two steels, but in the third steel it may be in excess.

This example explains the problems that appeared while describing retained δ-ferrite in steels using the equivalent concentration method.

Conclusions

1. It has been shown that the δ-ferrite fraction retained in the cast metal is determined, not only by its thermodynamic stability during solidification of liquid steel and cooling of solid steel, but also by its cooling rates in the temperature ranges of the existence of δ-ferrite and austenite.

The combined knowledge of the thermodynamic and kinetic δ-ferrite behavior will be useful for developing methods for increasing the crack resistance of steel in the presence of an optimal amount of δ-ferrite during hot plastic deformation or welding, as well as subsequent austenitization of the structure to minimize or eliminate δ-ferrite in the finished metal.

2. The patterns of the influence of the steel chemical composition and its cooling rate in the temperature ranges ΔT_δ, ΔT_{tech}, ΔT_γ on the retained δ-ferrite fraction and its morphology in the base metal and weld have been established.

2a. The cooling rate during solidification of steel and its subsequent cooling in the solid state does not have a decisive influence on the δ-ferrite fraction retained in the ingots. At high cooling rates of the melt during crystallization, the fraction of the δ-ferrite is much lower than the equilibrium level, since it does not have time to fully form. However, high cooling rates of solid metal limit the completeness of transformation of the previously formed δ-ferrite. At the low cooling rates of the melt during crystallization, the amount of δ-ferrite may be close to the equilibrium value, but with subsequent slow cooling of the solid metal it will completely transform to austenite.

2b. The inclination angle of the ascending straight line of δ-ferrite fraction from the edge of the ingot to its center is determined by its transformation degree that depends on the cooling rate, as well as thermodynamic stability (which depends on the steel composition and is determined by the previously developed criteria ΔT_δ, ΔT_{tech}, ΔT_γ, $\Delta(\delta)$).

2c. The morphology of δ-ferrite evolves from globular and vermicular to lacy during the transition from the edge to the center of ingots cast in metal molds. Mainly, the vermicular morphology remains over its entire cross section in the ingot obtained using the sand mold. The δ-ferrite formation of one morphology or another depends on the ratio of its nucleation and growth rates during crystallization and solidification, as well as the completeness of transformation into austenite upon cooling in solid steel.

3. Multivariate models have been obtained that adequately describe the δ-ferrite fraction retained in steel depending on its composition and cooling rate. These models describe well not only the results of this work, but also experimental data known from the literature and obtained using welding consumables that are similar in composition. A systematic error was established in the description of literature data using chromium and nickel equivalents. This error is due to the fact that the same equivalents can be obtained by a combination of different

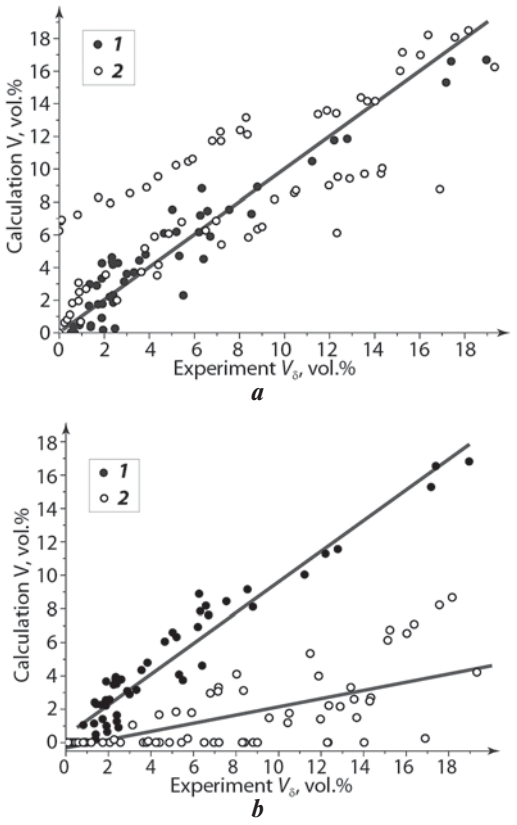

Fig. 7. Scatter diagram for the δ-ferrite volume fraction, V_δ: calculated vs. experimentally measured. Steel composition is in wt.% (*a*) and in chromium and nickel equivalents (*b*): *1* — this paper data; *2* — literature data [34]

concentrations of the same alloying elements, where the fraction of δ-ferrite retained in steel can vary significantly.

REFERENCES

1. Kalinin G. Yu., Mushnikova S. Yu., Nesterova E. V., Fomina O. V., Kharkov A. A. Research of structure and properties of a high-strength corrosion-resistant nitrogen steel C0.04Cr20Ni6Mn11Mo2NVNb. *Voprosy Materialovedenia (Materials Science Issues)*. 2006. No. 1 (45). p. 45–54.
2. Blinov G. Yu., Pojmenov I. L., Kulikova O. I., Karelin F. R., Shurygina I. A., Glebov V. V., Kalenihin Yu. N. Influence of hot deformation on structure and mechanical properties of nitrogen nonmagnetic steels. Structure and Physicomechanical Properties of Nonmagnetic Steels. Moscow: Science, 1986. p. 30–33.
3. Kaputkina L. M., Svyazhin A. G., Smarygina I. V., Kindop V. E. Influence of nitrogen and copper on hardening of austenitic chromium-nickelmanganese stainless steel. *CIS Iron and Steel Review*. 2016. Vol. 12. pp. 30–34.
4. Pickering F. B. Physical Metallurgy and the Design of Steels. London. Applied Science Publishers. 1978. 275 p.
5. Kujanpaa V. P., David S. A., White C. L. Formation of Hot Cracks in Austenitic Stainless Steel Welds — Solidification Cracking. *Welding Research Supplement*. 1986. No. 204. pp. 203–212.
6. Demk H. Deformation under Hot Working Conditions. London: The Iron and Steel Institute. 1968. 135 p.
7. Kane R. H. The Hot Deformation of Austenite. Pergamon Press. 1977. 457 p.
8. Brooks J. A., Thompson A. W., Williams J. C. A fundamental study of the beneficial effects of δ-ferrite in reducing weld cracking. *Welding Journal*. 1984. No. 3. pp. 71–83.
9. Priceputu I. L., Moisa B., Chiran A., Nicolescu G., Bacinschi Z. Delta ferrite influence in AISI 321 stainless steel welded tubes. *The Scientific Bulletin of Valahia University: Materials and Mechanics*. 2011. No. 6 (year 9). pp. 87–96.
10. Schaffler A. I. Constitution diagram for stainless steel weld metal. *Metal Progress*. 1949. No. 56. pp. 680–680.
11. DeLong W. T., Ostorm G. A., Szumachowski E. R. Measurement and calculation of ferrite in stainless steel weld metal. *Welding Journal*. 1956. No. 35 (11). pp. 521–528.
12. Speidel M. High Nitrogen Steels. *Proceedings of the 10th International Conference on High Nitrogen Steels*. 2009. p. 121.
13. Kazakov A. A., Shakhmatov A. V., Kolpishon E. Yu. Cast structure and an inheritance of high chromium steel with nitrogen. *Heavy Mechanical Engineering*. 2015. No. 1-2. p. 19–24.
14. Kazakov A. A., Oryshchenko A. S., Fomina O. V., Zhitenev A. I., Vihareva T. V., Control of the δ-ferrite origin in nitrogenous chromium nickel manganese steels. *Voprosy materialovedenia (Materials Science Issues)*. 2017. No. 1(89). pp. 7–12.
15. Kazakov A. A., Fomina O. V., Zhitenev A. I., Melnikov P. V. Physico-chemical fundamentals of controlling the δ-ferrite origin while welding by austenitic-ferritic materials. *Voprosy materialovedenia (Materials Science Issues)*. 2018. No. 4 (96). pp. 42–52.
16. David S. A. Ferrite Morphology and Variations in Ferrite Content in Austenitic Stainless Steel Welds. *Welding Research Supplement*. 1981. April. pp. 63-71.
17. Suutala N., Takalo T., Moisio T. The Relationship Between Solidification and Microstructure in Austenitic and Austenitic-Ferritic Stainless Steel Weld. *Metallurgical Transactions*. 1979. Vol. 10. Issue 4. pp. 512-514.
18. TU 14-1-2921-80. Welding steel wire. Grade SV-C0.01Cr19Ni11Mo4V (EP647).
19. Kazakov A, Kiselev D. Industrial Application of Thixomet. *Metallography, Microstructure, and Analysis*. 2016. Vol. 5. Iss.4. pp. 294-301. DOI 10.1007/s13632-016-0289-6.
20. Bale C., Bélisle E., Chartrand P., Decterov S., Eriksson G., Hack K., Jung I.-H., Kang Y.-B., Melançon J., Pelton A., Robelin C., Petersen S. FactSage Thermochemical Software and Databases — Recent Developments. *Calphad-computer Coupling of Phase Diagrams and Thermochemistry*. 2009. Vol. 33. pp. 295–311.
21. Golod V. M. Theory and computer analysis of foundry processes. Saint-Petersburg: Peter the Great St. Petersburg Polytechnic University. 2018. 243 p.
22. Vitek J. M., David S. A. The Sigma Phase Transformation in Austenitic Stainless Steels. *Welding Research Supplement*. 1986. April. pp. 106–112.
23. Leone G. L., Kerr H. W. The Ferrite to Austenite Transformation in Stainless Steels. *Welding Research Supplement*. 1980. January. pp. 13–22.
24. Kokawa H., Kuwana T., Yamamoto A. Crystallographic Characteristics of Delta Ferrite Transformations in f 304L Weld Metal at Elevated Temperatures. *Welding Research Supplemen*t. 1989. March. pp. 92–101.
25. Fukumoto, S., Iwasaki, Y., Motomura, H., Fukuda, Y. Dissolution behavior of -ferrite in Continuously Cast Slabs of SUS304 during Heat Treatment. *ISIJ International*. 2012. Vol. 52. No. 1. pp. 74–79.
26. Saied M. Experimental and numerical modeling of the dissolution of delta ferrite in the Fe–Cr–Ni system: application to the austenitic stainless steels. Materials University Grenoble. Alpes. 2016. p. 220.
27. David S. A., Vitek J. M., Hebble T. L. Effect of Rapid Solidification on Stainless Steel Weld Metal Microstructure and Its Implications on the Schaeffler Diagram. *Welding Research Supplement*. 1987. September. pp. 289-300.
28. Elmer J. W., Allen S. M., Eagar T. W. Microstructural Development during Solidification of Stainless Steel Alloys. *Metallurgical Transaction*. 1989. Vol. 20A. p. 2117–2131.
29. Inoue H., Koseki T. Clarification of Solidification Behaviors in Austenitic Stainless Steels Based on Welding Process. *Nippon steel technical report*. 2007. No. 95. pp. 62–70.
30. Folmer M. Kinetics of new phase formation. Moscow: Science. 1986. 208 p.
31. Koumatos K., Muehlemann A. A theoretical investigation of orientation relationships and transformation strains in steels. *Acta Crystallization*. 2017. No. 73. pp. 115–123.
32. Lifshitz I. M., Slyozov V. V. The kinetics of precipitation from supersaturated solid solutions. *Journal of Physics and Chemistry of Solids*. 1961. Vol. 19. No. 1-2. pp. 35–50.
33. Wagner C. Theorie der alterung von niderschlagen durch umlösen (Ostwald Reifung). *Zeitschrift für Elektrochemie*. 1961. Vol. 65. pp. 581–591.
34. Valiente Bermejo M.A. A Mathematical Model to Predict δ-Ferrite Content in Austenitic Stainless Steel Weld Metals. *Welding in the World*. 2012. Vol. 56. pp. 48–68.